A&A 535, A35 (2011)
DOI: 10.1051/0004-6361/201117550

Astronomy & Astrophysics

Radiative transfer with *J*-state interference in a two-term atom

Partial frequency redistribution in the non-magnetic case

H. N. Smitha[1], K. N. Nagendra[1], M. Sampoorna[1], and J. O. Stenflo[2,3]

[1] Indian Institute of Astrophysics, Koramangala, Bangalore, India
e-mail: [smithahn;knn;sampoorna]@iiap.res.in
[2] Institute of Astronomy, ETH Zurich, 8093 Zurich, Switzerland
e-mail: stenflo@astro.phys.ethz.ch
[3] Istituto Ricerche Solari Locarno, Via Patocchi, 6605 Locarno-Monti, Switzerland

Received 23 June 2011 / Accepted 29 August 2011

ABSTRACT

Context. Quantum interference phenomena play a fundamental role in the formation of linear polarization that arises from scattering processes in multiplets of the solar spectrum. In particular, the J-state interference between different line components of a multiplet (arising from transitions in a two-term atom) produces significant effects in the linearly polarized spectra.
Aims. We aim to solve the polarized radiative transfer equation for a two-term atom with the unpolarized lower term in isothermal slabs, including the effect of the interference between the upper J-states and partial frequency redistribution (PRD). We consider only the case of non-magnetic scattering.
Methods. The PRD matrix for the J-state interference derived in previous works is incorporated into the polarized transfer equation. The standard form of the two-level atom transfer equation is extended to a two-term atom. The transfer problem is then solved using a traditional polarized approximate lambda iteration method.
Results. We show how the PRD and the J-state interference together affect the shapes of the $(I, Q/I)$ profiles. We present the benchmark solutions for isothermal, constant-property slabs of a given optical thickness. We consider a hypothetical ${}^2S - {}^2P$ doublet produced by an $L = 0 \rightarrow 1 \rightarrow 0$ scattering transition with spin $S = 1/2$. We present the results in the form of Stokes $(I, Q/I)$ profiles for different values of (i) the line separation, (ii) optical thickness, (iii) thermalization parameter, and (iv) the continuum opacity.

Key words. line: formation – methods: numerical – polarization – radiative transfer – scattering – Sun: atmosphere

1. Introduction

The linearly polarized spectrum of the Sun, known as the "second solar spectrum", contains a wealth of information about the physics of light scattering on atoms. The interpretation of the shapes of the spectral lines in the second solar spectrum deepens our understanding of the physical processes taking place in the solar atmosphere, and also gives us a diagnostic tool for the determination of the solar magnetic fields. The solution of the polarized line transfer equation is necessary to interpret the shapes of the observed Stokes line profiles.

A quantum theory of upper J-state interference for frequency coherent scattering in the laboratory frame was formulated by Stenflo (1980, 1994, 1997). He introduced a wavelength-dependent polarizability factor $W_2(\lambda)$ to describe the phenomenon of quantum interference. Stenflo (1980) used this approach to model the observed scattering polarization signals in solar Ca II H and K lines. He applied the concept of the last scattering approximation for this purpose. The quantum interference theory of Stenflo (1980) was later included in the radiative transfer computations along with partial frequency redistribution (PRD) in Fluri et al. (2003, see also Holzreuter et al. 2006). A PRD matrix for the J-state interference in a two-term atom with unpolarized lower term and in the collisionless regime was derived in the atomic frame by Landi Degl'Innocenti et al. (1997) using a meta-level approach. Recently Smitha et al. (2011, hereafter P1) have derived the same PRD matrix starting from the Kramers-Heisenberg scattering formula. In P1 the expression for the laboratory frame PRD matrix is given. In the present paper we incorporate the PRD matrix derived in P1 into the polarized line transfer equation. For this purpose we generalize the vector version of the standard two-level atom NLTE line transfer equation (Mihalas 1978; Stenflo 1994) to the case of a two-term atom. We restrict our attention to the non-magnetic case.

It is necessary to distinguish between linear and non-linear NLTE radiative transfer problems for polarized radiation (e.g., Trujillo Bueno 2003). An example of a linear radiative transfer problem is the standard problem of scattering polarization and the Hanle effect in a gas of two-level atoms assuming that the lower level is unpolarized (e.g., Faurobert-Scholl 1991; Nagendra et al. 2002; Sampoorna et al. 2011, and the references cited therein). Examples of non-linear problems are the problems of scattering polarization and the Hanle effect in two-level or multilevel systems with atomic polarization in all levels (Trujiilo Bueno & Landi Deg'Innocenti 1997; Manso Sainz & Trujillo Bueno 2003, 2010). It is important to note that the two-term atom problem with an unpolarized lower term considered in this paper is essentially similar to the two-level atom problem without lower-level polarization. In other words, it is a linear problem that does not involve the simultaneous solution of the statistical equilibrium and the Stokes-vector transfer equations. All couplings between different components of the multiplet enter the transfer problem only through the PRD matrix.

Novel iterative schemes have been developed by Trujillo Bueno and coworkers (see Trujillo Bueno 2003, and references

therein to their previous works) to solve the complete frequency redistribution (CRD) polarized NLTE transfer equation in multi-level atoms with the polarization of all levels taken into account. A recent review by Trujillo Bueno (2011) describes the modeling of scattering polarization and the Hanle effect in some spectral lines. Reviews by Nagendra (2003a,b); Nagendra & Sampoorna (2009), and Nagendra et al. (2009) list several exact and approximate numerical methods of solving the polarized transfer equation for a two-level atom without lower level polarization. The polarized approximate lambda iteration (PALI) methods based on the Jacobi iterative scheme of Olson et al. (1986) have been developed to solve the two-level atom polarized transfer equation (see e.g. Nagendra 2003a). In the present paper we use one of the methods described in Nagendra & Sampoorna (2009) generalized appropriately to the case of a two-term atom to solve the J-state interference problem.

In Sect. 2 we discuss the transfer equation for a two-term atom model. In Sect. 2.1 we describe the decomposition of the Stokes vector $\boldsymbol{I}$ and source vector $\boldsymbol{S}$ into the two cylindrically symmetric components to cast the Stokes vector transfer equation in a reduced form. The numerical method of the solution is presented in Sect. 3. The computed results are discussed in Sect. 4. In Sect. 5 we present the conclusions.

2. The transfer equation

The radiation field in a non-magnetic plane parallel atmosphere with axisymmetric boundary conditions is axisymmetric. This axially symmetric polarized radiation field can be described by the two Stokes parameters I and Q (see Chandrasekhar 1950). The relevant line transfer equation for the problem of resonance scattering polarization may be written as

$$\frac{\partial}{\partial s}\begin{pmatrix} I \\ Q \end{pmatrix} = \begin{pmatrix} \epsilon_I \\ \epsilon_Q \end{pmatrix} - \begin{pmatrix} \eta_I & \eta_Q \\ \eta_Q & \eta_I \end{pmatrix}\begin{pmatrix} I \\ Q \end{pmatrix}. \tag{1}$$

Equation (1) is a special case of the general polarized transfer equation given by Eq. (8.2) of Landi Degl'Innocenti & Landolfi (2004, hereafter LL04), when the axial symmetry of the polarized radiation field is imposed. In Eq. (1) ∂s denotes the incremental distance along the ray; $\epsilon_{I,Q}$ are the emission coefficients in the Stokes vector $(I, Q)^{\mathrm{T}}$ basis; and $\eta_{I,Q}$ are the corresponding absorption coefficients. Under the assumption that the lower level of the transition is unpolarized, $\eta_Q = 0$. In this case the (2×2) absorption matrix becomes diagonal. For a line formed in the presence of a continuum

$$\eta_I = \eta_0 + k_c, \tag{2}$$

where η_0 is the line absorption coefficient, and k_c the continuum absorption coefficient. In the case of a standard two-level atom model, $\eta_0 = k_L\phi(x)$ where k_L is the frequency integrated line absorption coefficient, and $\phi(x)$ is the Voigt profile function for the reduced frequency x. The expression for η_0 in the particular case of a two-term atom can be derived starting from the general expressions for multi-term atom, given in LL04 (see Eq. (7.47a)). Alternatively, η_0 can also be derived by generalizing to the case of a two-term atom, the standard expression for intensity absorption coefficient of a two-level atom given in Mihalas (1978). Neglecting the induced emission term, it can be written as

$$\eta_0(J_a, J_b) = \frac{h\nu_{J_bJ_a}}{4\pi}B(J_a \to J_b)N(J_a)\phi(\nu_{J_bJ_a} - \nu), \tag{3}$$

where J_a and J_b are the total angular momentum quantum numbers of the lower and upper level respectively. $B(J_a \to J_b)$ is the Einstein's coefficient. $N(J_a)$ is the number density of atoms in the lower (J_a) level. $\nu_{J_bJ_a}$ is the line center frequency for the transition $J_b \to J_a$. $\phi(\nu_{J_bJ_a} - \nu)$ is the normalized Voigt profile function with line center frequency at $\nu_{J_bJ_a}$. Equation (3) can be generalized to the case of two-term atom by summing over various components of the multiplet, namely

$$\eta_M = \sum_{J_aJ_b} \eta_0(J_a, J_b). \tag{4}$$

A two-term atom is characterized by the orbital angular momentum L_a and L_b of the lower and upper terms respectively with spin S. Owing to $L - S$ coupling, a given (L, S) state splits into several J-states, with $|L - S| \le J \le |L + S|$. The coefficient $B(J_a \to J_b)$ is then related to $B(L_a \to L_b)$ through the expression

$$B(J_a \to J_b) = B(L_a \to L_b)(2L_a + 1)(2J_b + 1)\begin{Bmatrix} L_b & L_a & 1 \\ J_a & J_b & S \end{Bmatrix}^2, \tag{5}$$

(see Eqs. (8.43) and (9.74) of Stenflo 1994). The populations of the lower J-levels are related to the populations of the lower L-term through the relation

$$N(J_a) = (2J_a + 1)\frac{N(L_a)}{(2S + 1)(2L_a + 1)}, \tag{6}$$

where the assumption of unpolarized lower term is made. Using Eqs. (3), (5), and (6) in Eq. (4), we obtain

$$\eta_M(\nu) = \frac{k_M}{(2S + 1)}\sum_{J_aJ_b}(2J_a + 1)(2J_b + 1) \times \begin{Bmatrix} L_b & L_a & 1 \\ J_a & J_b & S \end{Bmatrix}^2 \phi(\nu_{J_bJ_a} - \nu), \tag{7}$$

where

$$k_M = \frac{h\nu_{J_aJ_b}}{4\pi}N(L_a)B(L_a \to L_b) \tag{8}$$

is the frequency-integrated absorption co-efficient of the entire multiplet. In the case of an $L = 0 \to 1 \to 0$ scattering transition with $S = 1/2$

$$\eta_M(\nu) = k_M\left[\frac{2}{3}\,\phi(\nu_{\frac{3}{2}\,\frac{1}{2}} - \nu) + \frac{1}{3}\,\phi(\nu_{\frac{1}{2}\,\frac{1}{2}} - \nu)\right]. \tag{9}$$

An expression analogous to that of the two-level atom can be recovered by introducing a combined profile function that for ${}^2S \to {}^2P \to {}^2S$ doublet is given by

$$\phi(x) = \left[\frac{2}{3}\,\phi(\nu_{\frac{3}{2}\,\frac{1}{2}} - \nu) + \frac{1}{3}\,\phi(\nu_{\frac{1}{2}\,\frac{1}{2}} - \nu)\right]. \tag{10}$$

Notice that the combined profile function $\phi(x)$ is a weighted sum of Voigt profiles of the two lines of the doublet. For the more general case of a $L_a \to L_b \to L_a$ scattering transition with spin S, Eq. (7) has to be used to obtain explicit expressions for the corresponding combined profile function. The combined profile function $\phi(x)$ can also be derived using the theoretical framework of Stenflo (1997, see his Sect. 3.1). It is also implicitly contained in the general definition for the intensity absorption coefficient for a multi-term atom given in LL04.

Defining the optical depth scale as $\mathrm{d}\tau = -k_M \mathrm{d}z$, we can rewrite Eq. (1) as

$$\mu \frac{\partial \boldsymbol{I}(\tau,x,\mu)}{\partial \tau} = (\phi(x)+r)[\boldsymbol{I}(\tau,x,\mu) - \boldsymbol{S}(\tau,x,\mu)], \tag{11}$$

where $\mu = \cos\theta$ with θ being the colatitude with respect to the atmospheric normal. $\boldsymbol{I} = (I,Q)^{\mathrm{T}}$ is the Stokes vector. $\boldsymbol{S} = (S_I, S_Q)^{\mathrm{T}}$ is the total source vector given by

$$S_{I,Q} = \frac{\epsilon_{I,Q}}{\eta_I}. \tag{12}$$

x is the scattered frequency in Doppler width units. r is the ratio of continuum to the frequency-integrated line absorption coefficient. The positive Stokes Q represents electric vector vibrations perpendicular to the solar limb.

The total source vector $\boldsymbol{S}$ is given by

$$\boldsymbol{S}(\tau,x,\mu) = \frac{\phi(x)\boldsymbol{S}_l(\tau,x,\mu) + r\boldsymbol{S}_{\mathrm{c}}}{\phi(x)+r}, \tag{13}$$

where the unpolarized continuum source vector $\boldsymbol{S}_{\mathrm{c}} = B\boldsymbol{U}$, with B being the Planck function and $\boldsymbol{U} = (1,0)^{\mathrm{T}}$. The line source vector for a two-term atom has the form

$$\boldsymbol{S}_l(\tau,x,\mu) = \epsilon B\boldsymbol{U} + \frac{1}{\phi(x)}\int_{-\infty}^{+\infty}\mathrm{d}x' \times \int_{-1}^{1}\frac{\mathrm{d}\mu'}{2}\mathbf{R}(x,\mu,x',\mu')\boldsymbol{I}(\tau,x',\mu'), \tag{14}$$

where x' is the incoming frequency in Doppler width units and $\epsilon = \Gamma_I/(\Gamma_I+\Gamma_R)$ is the photon destruction probability per scattering with Γ_I and Γ_R being the inelastic and radiative de-excitation rates of the upper term L_b. We assume that Γ_I and Γ_R are the same for all fine structure levels of the upper term. The non-magnetic two-term atom redistribution matrix is given by Eq. (26) of P1.

Note that the redistribution matrix derived in P1 depends on incoming and outgoing ray directions $\boldsymbol{n}'(\theta',\varphi')$ and $\boldsymbol{n}(\theta,\varphi)$ which are defined with respect to the atmospheric normal. The angular dependence appears not only in the phase matrix part of the redistribution matrix, but also in the redistribution functions. To simplify the problem, following Rees & Saliba (1982), we here replace the angle-dependent redistribution functions by their angle-averaged analogues. The angle-averaged functions can be computed from the angle-dependent functions by integrating over the scattering angle between the incident and scattered ray (cf. Bommier 1997).

Owing to the azimuthal symmetry of the problem, one can then integrate the phase matrix part of the redistribution matrix over the azimuths φ' of the incoming radiation to obtain $\mathbf{R}(x,\mu,x',\mu')$, which is given by

$$\mathbf{R}_{ij}(x,\mu;x',\mu') = \sum_K \mathcal{R}^K(x,x')\widetilde{\mathcal{T}}^K_0(i,\mu)\widetilde{\mathcal{T}}^K_0(j,\mu'), \tag{15}$$

where $i,j = 0,1$ and $\widetilde{\mathcal{T}}^K_0(i,\mu)$ are given by Eq. (28) of Frisch (2007) with $K = 0,2$. $\widetilde{\mathcal{T}}^K_Q(i,\mu)$ are related to the irreducible spherical tensors for polarimetry $\mathcal{T}^K_Q(i,\boldsymbol{n})$ introduced by Landi Degl'Innocenti (1984), through

$$\mathcal{T}^K_Q(i,\boldsymbol{n}) = \widetilde{\mathcal{T}}^K_Q(i,\mu)\mathrm{e}^{\mathrm{i}Q\varphi}, \tag{16}$$

with Q taking values $-K \le Q \le +K$.

The redistribution function components $\mathcal{R}^K(x,x')$ are given by

$$\begin{aligned}\mathcal{R}^K(x,x') = {} & \frac{3(2L_b+1)}{2S+1}\sum_{J_aJ_fJ_bJ_{b'}}(-1)^{J_f-J_a}\cos\beta_{J_{b'}J_b} \\ & \times[\cos\beta_{J_{b'}J_b}(h^{\mathrm{II}}_{J_b,J_{b'}})_{J_aJ_f} - \sin\beta_{J_{b'}J_b}(f^{\mathrm{II}}_{J_b,J_{b'}})_{J_aJ_f}] \\ & \times(2J_a+1)(2J_f+1)(2J_b+1)(2J_{b'}+1) \\ & \times\begin{Bmatrix} L_a & L_b & 1 \\ J_b & J_f & S\end{Bmatrix}\begin{Bmatrix} L_a & L_b & 1 \\ J_b & J_a & S\end{Bmatrix}\begin{Bmatrix} L_a & L_b & 1 \\ J_{b'} & J_f & S\end{Bmatrix}\begin{Bmatrix} L_a & L_b & 1 \\ J_{b'} & J_a & S\end{Bmatrix} \\ & \times\begin{Bmatrix} 1 & 1 & K \\ J_{b'} & J_b & J_a\end{Bmatrix}\begin{Bmatrix} 1 & 1 & K \\ J_{b'} & J_b & J_f\end{Bmatrix}.\end{aligned} \tag{17}$$

In Eq. (17), $L_{a,b}$ are the orbital angular momentum quantum numbers of the lower and upper terms respectively and S is the spin. $J_{a,f}$ are the total angular momentum quantum numbers of the fine structure levels of the lower term and $J_{b,b'}$ are the total angular momentum quantum numbers of the fine structure levels of the upper term. The auxiliary functions $(h^{\mathrm{II}}_{J_b,J_{b'}})_{J_aJ_f}$ and $(f^{\mathrm{II}}_{J_b,J_{b'}})_{J_aJ_f}$ are defined in Eqs. (14) and (15) of P1 but are used here for the non-magnetic case and with angle-averaged redistribution functions of type-II. The angle $\beta_{J_{b'}J_b}$ is defined in Eq. (10) of P1.

2.1. Decomposition of the Stokes vectors

In general the source vector $\boldsymbol{S}$ and the Stokes vector $\boldsymbol{I}$ depend on the colatitude θ of the radiation field. Computationally it is advantageous to work in a reduced basis, where the source vector components do not depend on θ (see for e.g. Faurobert-Scholl et al. 1997). Transformation of the Stokes vectors to such a reduced basis is referred to as the "decomposition" of the Stokes vectors. Using $\mathcal{T}^K_Q(i,\boldsymbol{n})$, Frisch (2007) has presented an elegant decomposition technique for the case of the Hanle effect. It is straightforward to apply this decomposition technique to the problem at hand. Here we briefly present a few important equations of this decomposition.

Let us denote $I_i = (I,Q)$ with $i = 0,1$ as the components of the Stokes vector. For the cylindrically symmetric case, the components I_i of the Stokes vector can be decomposed in terms of two irreducible components $\mathcal{I}^K_Q$ as follows

$$I_i(\tau,x,\mu) = \sum_{K=0,2}\widetilde{\mathcal{T}}^K_0(i,\mu)\mathcal{I}^K_0(\tau,x,\mu). \tag{18}$$

Similarly, the source vector $\boldsymbol{S}$ can be decomposed in terms of two cylindrically symmetric components $\mathcal{S}^K_0$, which become independent of even μ. $\widetilde{\mathcal{T}}^K_0(i,\mu)$ are real for $K = 0,2$ and $i = 0,1$, and thus $\mathcal{I}^K_0$ and $\mathcal{S}^K_0$ are also real.

For the non-magnetic case, we define the two-component vectors $\boldsymbol{\mathcal{I}} = \{\mathcal{I}^0_0, \mathcal{I}^2_0\}^{\mathrm{T}}$ and $\boldsymbol{\mathcal{S}} = \{\mathcal{S}^0_0, \mathcal{S}^2_0\}^{\mathrm{T}}$. The transfer equation for $\boldsymbol{\mathcal{I}}$ can now be written as

$$\mu\frac{\partial \boldsymbol{\mathcal{I}}(\tau,x,\mu)}{\partial\tau} = (\phi(x)+r)[\boldsymbol{\mathcal{I}}(\tau,x,\mu) - \boldsymbol{\mathcal{S}}(\tau,x)]. \tag{19}$$

The irreducible total source vector takes the form

$$\boldsymbol{\mathcal{S}}(\tau,x) = \frac{\phi(x)\boldsymbol{\mathcal{S}}_l(\tau,x) + r\boldsymbol{\mathcal{G}}(\tau)}{\phi(x)+r}, \tag{20}$$

where $\boldsymbol{\mathcal{G}}(\tau) = \{B,0\}^{\mathrm{T}}$ is the primary source vector. The irreducible line source vector is given by

$$\boldsymbol{\mathcal{S}}_l(\tau,x) = \epsilon\boldsymbol{\mathcal{G}}(\tau) + \int_{-\infty}^{+\infty}\frac{\widetilde{\mathcal{R}}(x,x')}{\phi(x)}\boldsymbol{\mathcal{J}}(\tau,x')\mathrm{d}x'. \tag{21}$$

Here $\widetilde{\mathcal{R}}(x, x')$ is a (2×2) diagonal matrix with elements $\widetilde{\mathcal{R}} = \mathrm{diag}\,(\mathcal{R}^0, \mathcal{R}^2)$, where $\mathcal{R}^K$ are defined in Eq. (17).

The mean intensity $\mathcal{J}(\tau, x)$ for the non-magnetic case is a two-component vector defined by

$$\mathcal{J}(\tau, x) = \frac{1}{2}\int_{-1}^{+1} \mathbf{\Psi}(\mu')\mathcal{I}(\tau, x, \mu')\mathrm{d}\mu'. \tag{22}$$

The elements of the (2×2) matrix $\mathbf{\Psi}(\mu)$ are given in LL04 (see also Appendix A of Frisch 2007). In the following sections, for notational brevity we specify the functional dependence of physical quantities as subscripts.

3. Numerical method of solution

We solve the polarized line radiative transfer equation for non-magnetic (Rayleigh) scattering on a two-term atom including the effects of J-state interference given in Eq. (19). We use the PALI method developed in Nagendra & Sampoorna (2009) appropriately extended to handle the present problem. In the following subsections we briefly describe this iterative technique.

3.1. The iteration scheme

The formal solution of the transfer equation may be stated in terms of the full lambda operator as

$$\mathcal{J}_x = \mathbf{\Lambda}_x[\mathcal{S}_x], \tag{23}$$

where $\mathbf{\Lambda}_x$ operates on the quantity within [ ]. By defining a local monochromatic approximate Lambda operator $\mathbf{\Lambda}^*_x$ as

$$\mathbf{\Lambda}_x = \mathbf{\Lambda}^*_x + \delta\mathbf{\Lambda}_x = \mathbf{\Lambda}^*_x + (\mathbf{\Lambda}_x - \mathbf{\Lambda}^*_x), \tag{24}$$

we can set up an iterative scheme to compute the source vectors, namely

$$\mathcal{S}^{(n+1)}_x = \mathcal{S}^{(n)}_x + \delta\mathcal{S}^{(n)}_x, \tag{25}$$

$$\mathcal{S}^{(n+1)}_{l,x} = \mathcal{S}^{(n)}_{l,x} + \delta\mathcal{S}^{(n)}_{l,x}, \tag{26}$$

where the superscript (n) refers to the nth iteration step. From Eqs. (24) and (25) it follows, by keeping only terms up to the first order, that

$$\mathcal{J}^{(n+1)}_x \approx \mathcal{J}^{(n)}_x + \mathbf{\Lambda}^*_x[\delta\mathcal{S}^{(n)}_x]. \tag{27}$$

Inserting Eqs. (21) and (27) into Eq. (26), we obtain a set of linear equations for the corrections to the line source vector $\delta\mathcal{S}^{(n)}_{l,x}$:

$$\delta\mathcal{S}^{(n)}_{l,x} - \int_{-\infty}^{+\infty} \frac{\widetilde{\mathcal{R}}_{x,x'}}{\phi_x} p_{x'}\mathbf{\Lambda}^*{}_{x'}[\delta\mathcal{S}^{(n)}_{l,x'}]\mathrm{d}x' = \boldsymbol{r}^{(n)}_x. \tag{28}$$

In deriving the above equation we have used the relation

$$\mathbf{\Lambda}^*_x[\delta\mathcal{S}^{(n)}_x] = p_x\mathbf{\Lambda}^*_x[\delta\mathcal{S}^{(n)}_{l,x}], \tag{29}$$

where $p_x = \phi_x/(\phi_x + r)$ is a scalar quantity defining the fractional line absorption and Λ^*_x is a linear operator. The frequency dependent residual vector is given by

$$\boldsymbol{r}^{(n)}_x = \mathcal{S}^{(n)}_{\mathrm{FS},l,x} - \mathcal{S}^{(n)}_{l,x}. \tag{30}$$

The formal line source vector is obtained from

$$\mathcal{S}^{(n)}_{\mathrm{FS},l,x} = \epsilon\mathcal{G}(\tau) + \int_{-\infty}^{+\infty} \frac{\widetilde{\mathcal{R}}_{x,x'}}{\phi(x)}\mathcal{J}^{(n)}_{x'}\mathrm{d}x', \tag{31}$$

where the mean intensity $\mathcal{J}^{(n)}_x = \mathbf{\Lambda}_x[\mathcal{S}^{(n)}_x]$ is computed using a short characteristic formal solver.

3.2. Calculation of the source vector corrections

The important step of the iterative method is the calculation of the source vector corrections $\delta\mathcal{S}^{(n)}_{l,x}$. Here we use the frequency by frequency (FBF) method of Paletou & Auer (1995) to compute these corrections, suitably generalized to the vector case (see also Sampoorna et al. 2008). The system of linear equations (Eq. (28)) can be organized in the matrix form as

$$\mathbf{A}\delta\mathcal{S}_l = \boldsymbol{r}, \tag{32}$$

where the vector $\boldsymbol{r}$ is the right-hand side of Eq. (28). At each depth point, for the non-magnetic case, $\mathbf{A}$ is a $2N_x \times 2N_x$ matrix with N_x the number of frequency points, and $\boldsymbol{r}$ has a length $2N_x$. Each element of $\mathbf{A}$ corresponding to a given value of x and x' is a 2×2 block denoted by $\mathbf{A}^2$, which is given by

$$\mathbf{A}^2_{ij} = \delta_{i,j}\mathbf{E} - \frac{\widetilde{\mathcal{R}}_{i,j}}{\phi_i} p_j\mathbf{\Lambda}^*_j; \quad i, j = 1, 2, 3, ..., N_x. \tag{33}$$

Here $\mathbf{E}$ is the 2×2 identity matrix. $\delta_{i,j}$ is the Kronecker's delta. The indices (i, j) refer to discretized values of (x, x'), respectively. The matrix $\mathbf{A}$ is computed only once because it does not change during the iteration.

We note that the polarized radiative transfer equation and its method of solution presented in Sects. 2 and 3 are valid for any scattering transition of the type $L_a \rightarrow L_b \rightarrow L_a$ in a two-term atom. In Sect. 4 we present the results only for an $L = 0 \rightarrow 1 \rightarrow 0$ scattering transition with $S = 1/2$, which corresponds to a doublet. The absorption profile function $\phi(x)$ for this doublet is given in Eq. (10).

4. Results and discussions

In this section we present the emergent Stokes profiles obtained by solving the polarized line radiative transfer equation for a hypothetical doublet at 5000 Å and 5001 Å. They arise from an $L = 0 \rightarrow 1 \rightarrow 0$ scattering transition with spin $S = 1/2$ and include the effects of J-state interference. We consider isothermal constant property slabs with a given optical thickness T to perform the tests. T is varied from optically thin ($T \ll 1$) to optically thick ($T \gg 1$) slabs. The slabs are assumed to be self-emitting unless stated otherwise. The slabs are illuminated at the lower boundary when they are assumed as pure scattering media ($\epsilon = 0$). The atmospheric model parameters used for the computations are represented by (T, a, ϵ, r), where a is the damping parameter. The Planck function B is taken as unity. The Doppler width for both lines are assumed to be the same and equal to 0.025 Å. The grid resolution in the physical variables is given by the values of $(N_\mathrm{d}, N_x, N_\mu)$. The quantity N_d represents the number of depth points per decade in a logarithmically spaced τ-grid. Unless stated otherwise, the first depth point $\tau_{\min} = 10^{-2}$ and $N_\mathrm{d} = 5$. The frequency grid points are very closely and equally spaced near the cores of the two lines as well as in between the two lines, and sparsely but equally spaced in the wings of the two lines. The total number of frequency points $N_x = 308$. We use a Gauss-Legendre quadrature for colatitude θ (μ) with $N_\mu = 5$ points.

4.1. Scattering in optically thin slabs

To mimic a single scattering event from a radiative line transfer problem with PRD, we consider an optically thin slab illuminated at the lower boundary by an unidirectional unpolarized

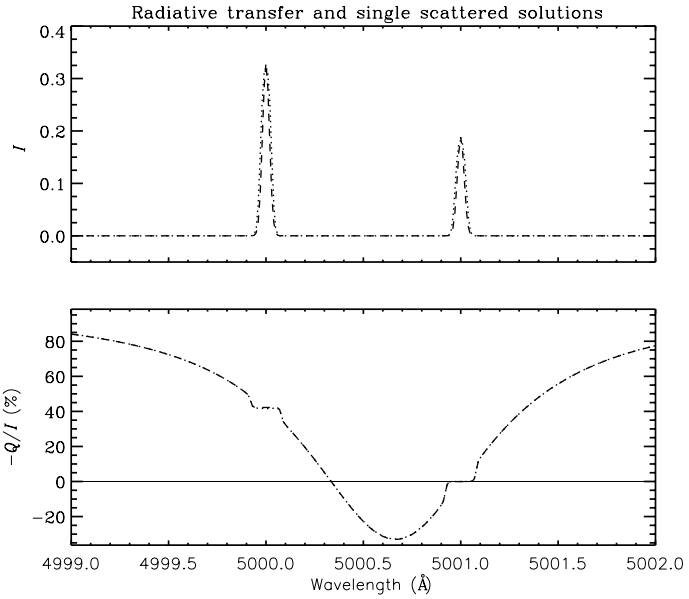

Fig. 1. Emergent Stokes profiles formed in an optically thin medium shown as a function of wavelength for nearly tangential emergence $\mu = 0.47 \times 10^{-2}$ (dotted line). The model parameters are $T = 2 \times 10^{-2}, a = 10^{-3}, \epsilon = 0$, and $r = 0$. A nearly vertical beam of radiation incident at $\mu' = 0.995$ is used as the lower boundary condition. In this case, the intensity is scaled up by a factor of 102 for comparison with the single scattered solution. The dashed line shows the emergent Stokes profiles computed for the single scattering case with the same value of scattering angle.

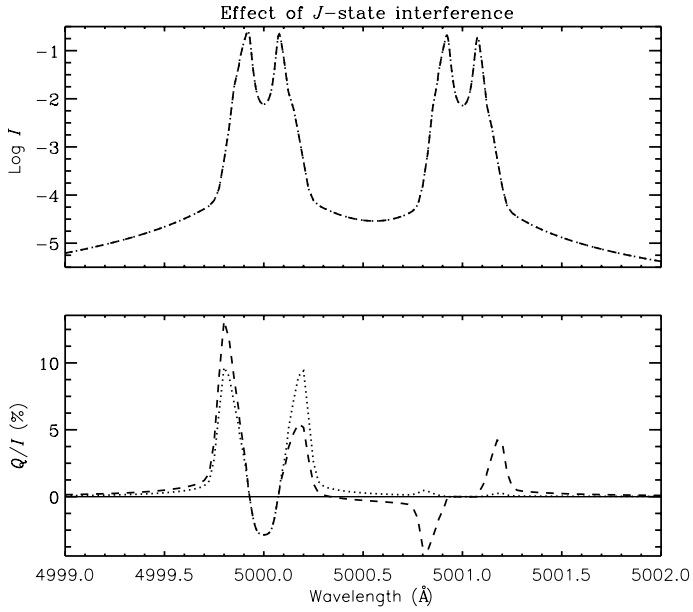

Fig. 2. Emergent Stokes profiles computed without J-state interference (dotted line) and with J-state interference (dashed line) at $\mu = 0.047$ for an optical thickness $T = 2 \times 10^4$. The other model parameters are $(a, \epsilon, r) = (10^{-3}, 10^{-4}, 0)$.

beam of radiation, namely, $\boldsymbol{\mathcal{I}}(\tau = T, x', \mu' = 0.995) = \boldsymbol{U}$. The other parameters used are $(T = 2 \times 10^{-2}, a = 10^{-3}, \epsilon = 0, r = 0)$. The first depth point is $\tau_{\rm min} = 10^{-4}$ and $N_\mu = 17$. The optical thickness is chosen to be very small so that the emergent diffuse radiation field is dominated by single scattered photons. The choice of parameters $\epsilon = 0$ and $r = 0$ represents a purely scattering medium without any continuum absorption. In Fig. 1 we compare emergent profiles computed from the line transfer problem that mimics a nearly 84° single scattering event (dotted line) with the profiles computed for the exact 84° single scattering case (dashed line). The intensity computed from the transfer code has been scaled up by a factor of 102 (dotted line), to match with intensity obtained from the single scattering case. From Fig. 1 we see that the shape of the profiles computed with the transfer code are very similar to the profiles for the single scattering case. They are similar to the single scattered Q/I profiles of Stenflo (1980; see also Fig. 10.17 of LL04). This verifies that the **R** matrix has been correctly incorporated into the line transfer code. We plot $-Q/I$ only in Fig. 1 to facilitate a quick comparison with the corresponding single scattered profiles presented in Stenflo (1980; see also P1).

4.2. Comparison between Stokes profiles with and without J-state interference

Figure 2 shows a comparison between the Stokes profiles computed with and without the effects of J-state interference. The effects of J-state interference in a doublet (or even a multiplet) system can be neglected by simply setting $J_b = J_{b'}$ in the RHS of Eq. (17), so that there is only one summation over J_b. These profiles are plotted for an atmosphere with $T = 2 \times 10^4$, $a = 10^{-3}, \epsilon = 10^{-4}$, and $r = 0$. It is well known from the single line two-level atom transfer computations that owing to the effects of PRD, two symmetric wing peaks appear in the Q/I profiles on either side of the line center. These peaks are referred to as the PRD peaks. For a doublet without the effect of J-state interference, or in other words, two non-interacting lines, these symmetric PRD peaks are visible around the lines at 5000 Å and 5001 Å (see dotted line in Fig. 2). Q/I at the 5001 Å line (arising from the $1/2 \rightarrow 1/2 \rightarrow 1/2$ scattering transition) is zero because the polarizability factor W_2 is zero for this line. If one includes J-state interference effects between the two lines, the near wing PRD peaks around the 5000 Å line become asymmetric (see the dashed line). The amplitude of the PRD peak at 4999.8 Å is increased, whereas the amplitude of the PRD peak at 5000.2 Å is decreased. Moreover, the symmetric PRD peaks around 5001 Å are converted into anti-symmetric peaks by the J-state interference effects. The amplitudes of these peaks are also enhanced. Comparing the dotted line with the dashed line, it is evident that these effects are caused by J-state interference.

The prominent signature of the J-state interference is the sign reversal in Q/I in the region of interference between the two lines. This is clearly visible in the dashed line, which includes this effect, but not in the dotted line which represents the case of the non-interacting lines.

Though there are striking differences between the Q/I for the two cases – with and without J-state interference, the intensity I is unaffected by this phenomenon.

4.3. Effects of optical thickness T of the medium on the J-state interference

In Fig. 3 we present the Stokes profiles for slabs with different values of optical thickness T. For all examples, $T \geq 2 \times 10^2$ with the thermalization parameter $\epsilon = 10^{-4}$. The chosen values of T represent a wide variety of the scattering media ranging from those that are effectively thin ($\epsilon T = 2 \times 10^{-2}$, for $T = 2 \times 10^2$) to those that are effectively thick ($\epsilon T = 2 \times 10^4$, for $T = 2 \times 10^8$). The other model parameters are $(a = 10^{-3}, r = 0)$.

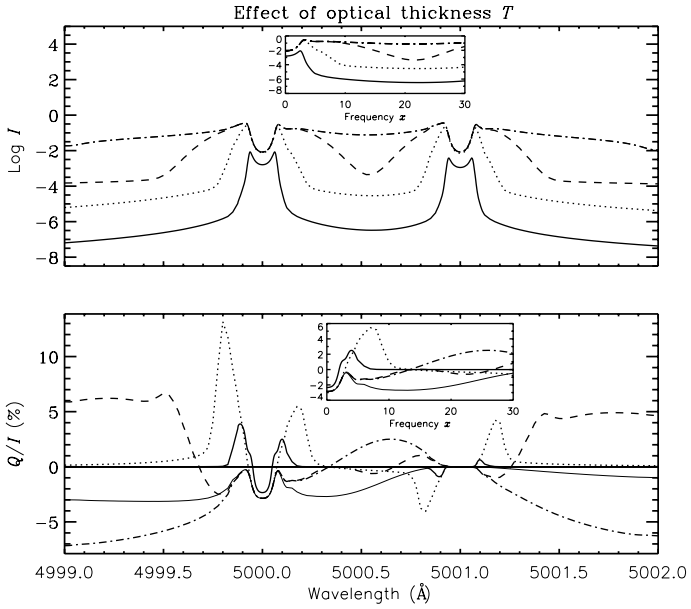

Fig. 3. Emergent Stokes profiles at $\mu = 0.047$ computed for optical thickness $T = 2 \times 10^2$ (thick solid line), $T = 2 \times 10^4$ (dotted line), $T = 2 \times 10^6$ (dashed line) and $T = 2 \times 10^8$ (dot-dashed line). The thin solid line represents a profile without J-state interference for $T = 2 \times 10^8$. The other model parameters are the same as in Fig. 2. The insets are plotted as functions of the non-dimensional frequency (x), measured from the line at 5000 Å to compare with the single line results (see Fig. 10 of Sampoorna et al. 2011).

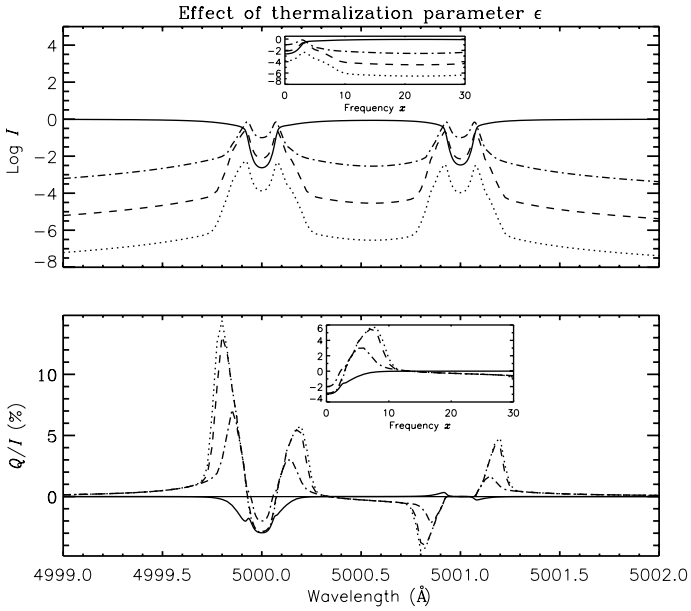

Fig. 4. Same as Fig. 3 but for various values of the thermalization parameter $\epsilon = 0$ (solid line), $\epsilon = 10^{-6}$ (dotted line), $\epsilon = 10^{-4}$ (dashed line) and $\epsilon = 10^{-2}$ (dot-dashed line). The remaining parameters are $(T, a, r) = (2 \times 10^4, 10^{-3}, 0)$.

The variation of I and Q/I with T in the case of a doublet is similar to that of a single-line case. This can be seen from the inset panels in I and Q/I in Fig. 3 and in turn comparing them with the left panel in Fig. 10 (dashed lines) of Sampoorna et al. (2011). In the inset panels I and Q/I are plotted as a function of the non-dimensional frequency (x), which is measured from the center of the line at 5000 Å. As the optical thickness increases, the magnitudes of Q/I at the PRD peaks initially increase and then decrease. This decrease is caused by the influence of multiple scattering. The thicker the atmosphere, the more isotropic is the radiation field because of multiple scattering. Accordingly, the polarization is reduced (see Rees 1978).

Furthermore, as T increases, the PRD peaks shift away from the line centers of the two lines. For $T = 2 \times 10^6$ and $T = 2 \times 10^8$, the PRD peaks occur far away from the centers of the two lines. For instance, at the wing frequencies between the two lines, the interference effects dominate over PRD-effects, resulting in suppression of the PRD peaks. Hence, there are no PRD peaks visible in between the two lines for these two values of T. However, their counterpart PRD peaks are visible on the outer sides of the two lines that are away from the region of interference between the two lines. For $T = 2 \times 10^8$ the PRD peaks occur so far out in the wings that they cannot be shown in the scale adopted for Fig. 3.

For $T = 2 \times 10^8$, an interesting feature is visible in the region of interference between the two lines. The Q/I profile displays a bump in the interference region between them (see the dot-dashed line). This behavior can be understood by comparing it with the thin solid curve that represents the result for the same model atmosphere, but without the effects of J-state interference, namely for the case of two non-interacting lines (shown only in the Q/I panel). The bump arises because of the sign reversal in Q/I that is in turn caused by the J-state interference effects. For two non-interacting lines, as seen from the thin solid curve, the Q/I between the two lines is negative. The J-state interference effects flip the sign of Q/I in this region which causes this bump, as seen in the dot-dashed curve. A smaller bump visible at 5000.8 Å for $T = 2 \times 10^6$ can also be understood in a similar way (the corresponding curve for two non-interacting lines is not shown in the figure).

4.4. Effects of the thermalization parameter ϵ on the J-state interference

In Fig. 4 we present the Stokes profiles for different values of the thermalization parameter ϵ. The optical thickness of the medium is fixed at $T = 2 \times 10^4$. The value of ϵ is varied from 10^{-2} to 0, which covers effectively thick to effectively thin slabs. The other model parameters are $a = 10^{-3}$ and $r = 0$.

For $\epsilon = 0$, there are no internal sources of photons. This is an example of a pure scattering medium. We give $I_0^0(\tau = T, x, \mu) = 1$ as the boundary condition at the lower boundary. In this case, the emergent intensity is an absorption profile.

The variation of I and Q/I with ϵ in the case of a doublet is similar to that of the single line case. This can be seen from the inset panels in I and Q/I in Fig. 4. As ϵ increases from 10^{-6} to 10^{-2}, the intensity increases and the degree of linear polarization Q/I decreases in the line core and near wings of both the lines. For $\epsilon \neq 0$, the emergent intensity profiles become self-reversed emission lines. This behavior is similar to that of the single line case as can be seen from the right panel in Fig. 10 (dashed lines) of Sampoorna et al. (2011).

It is worth noting that the wavelength region between 5000.3 Å to 5000.7 Å is insensitive to the variation in ϵ, except when $\epsilon = 0$ (in which case Q/I approaches zero). The J-state interference effects show up most prominently in this wavelength region in between the two lines. For $\epsilon = 0$, the emergent radiation in the wings approach the incident radiation which is unpolarized (see Sampoorna et al. 2008). The curve for two non-interacting lines (not shown in the figure) for this case nearly

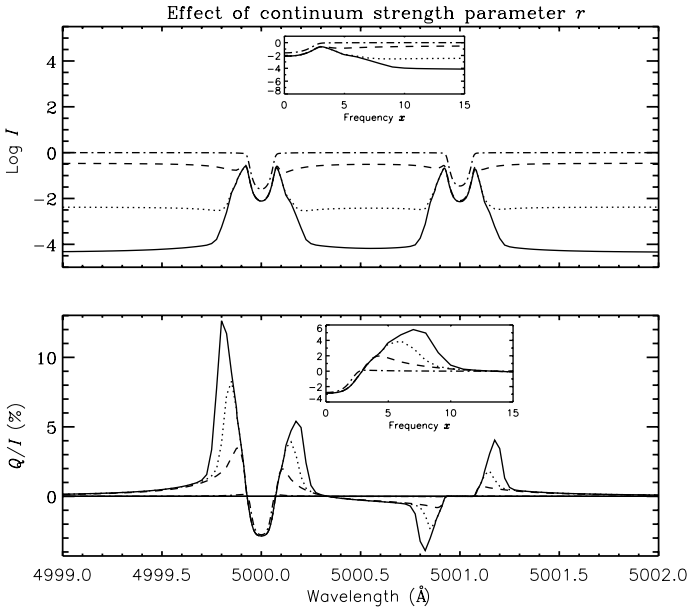

Fig. 5. Same as Fig. 3 but for different values of the continuum parameter $r = 10^{-10}$ (solid line), $r = 10^{-8}$ (dotted line), $r = 10^{-6}$ (dashed line) and $r = 10^{-4}$ (dot-dashed line). The other model parameters are $(T, a, \epsilon) = (2 \times 10^4, 10^{-3}, 10^{-4})$. The insets are plotted as functions of the non-dimensional frequency (x), measured from the line at 5000 Å to compare with the single line results (see Fig. 11 of Sampoorna et al. 2011).

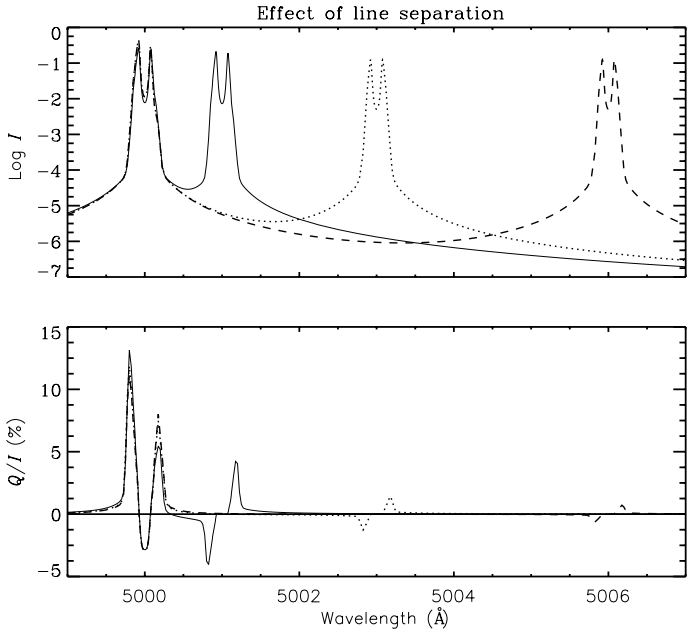

Fig. 6. Effect of line separation between the doublets. Three different line separations are chosen, namely 1 Å (solid line), 3 Å (dotted line), and 6 Å (dashed line). The model parameters are $(T = 2 \times 10^4, a = 10^{-3}, \epsilon = 10^{-4}, r = 0)$.

coincides with the curve including the effects of J-state interference (solid line) except for the two small PRD peaks on either side of the line at 5001 Å, which are slightly enhanced because of this effect, as discussed above.

4.5. Effect of the unpolarized background continuum on the J-state interference

The results shown in the previous sections were obtained without a background continuum ($r = 0$). In Fig. 5 we show the Stokes profiles for different values of the continuum strength r. The other model parameters are $(T = 2 \times 10^4, a = 10^{-3}, \epsilon = 10^{-4})$. r is varied from 10^{-10} to 10^{-4} in steps of 10^{-2}. When r increases, we observe a significant decrease in the amplitude of the near wing PRD peaks in Q/I. Also the J-state interference effects vanish for $r = 10^{-4}$ away from the line cores (see the dot-dashed line in Fig. 5). The insets in Fig. 5 show a behavior similar to the single line case seen in Fig. 11 (dashed lines) of Sampoorna et al. (2011). As r increases, the intensity profile evolves from a "self-reversed emission line" to an absorption line.

4.6. Effect of line separation between the doublets coupled through the J-state interference

In Fig. 6 we present the scattered Stokes profiles for three different values of the separation between the lines. The model parameters are $(T = 2 \times 10^4, a = 10^{-3}, \epsilon = 10^{-4}, r = 0)$. The line separations used are 1 Å, 3 Å and 6 Å (measured from the 5000 Å line). Evidently, the Q/I amplitudes of the near wing PRD peaks about the lines at 5001 Å, 5003 Å and 5006 Å decrease with the increase in line separation.

This behavior is expected, because the polarizability factor $W_2 = 0$ for the $1/2 \rightarrow 1/2 \rightarrow 1/2$ transition, producing no polarization at the line center. J-state interference together with PRD in scattering is responsible for polarization signals near the resonance frequency of this line component. As the separation of the $1/2 \rightarrow 1/2 \rightarrow 1/2$ component increases, the J-state interference effects naturally decrease, resulting in successively weaker signals. It is useful to note that although characteristic signals are generated near the $1/2 \rightarrow 1/2 \rightarrow 1/2$ resonance frequency, $Q/I = 0$ at the actual line center. As the figure shows, PRD along with the effects of J-state interference can indeed generate Q/I signals near the centers of multiplet components with $W_2 = 0$, but these signatures have an anti-symmetric shape with a zero crossing at the exact line center. These antisymmetric polarization signals can also be produced at the $1/2 \rightarrow 1/2 \rightarrow 1/2$ transition using CRD (see Trujillo Bueno et al. 2002; Casini & Manso Sainz 2005, where also the role of hyperfine structure and lower term polarization are investigated).

4.7. Comparison of the redistribution matrix approach with the quantum interference theory of Stenflo

In this section we compare our redistribution matrix approach and the quantum interference theory of Stenflo (1980; see also Stenflo 1997). The comparison is shown in Fig. 7. The solid line shows the profile computed with the exact J-state interference theory presented in Sect. 2. We refer to this as the redistribution matrix approach. The dotted line shows the profiles computed from an independent line transfer code. In this code, in place of $\mathcal{R}^K(x, x')$ we use

$$W_K(\nu)[R^{\mathrm{II-A}}(3/2 \rightarrow 1/2) + R^{\mathrm{II-A}}(1/2 \rightarrow 1/2)],$$

where $R^{\mathrm{II-A}}(J_b \rightarrow J_a)$ are the angle-averaged frequency redistribution functions of Hummer (1962) for the line with center frequency at $\nu_{J_b J_a}$ corresponding to the $J_b \rightarrow J_a$ transition. The polarizability factor $W_0(\nu) = 1$, and $W_2(\nu)$ is the frequency-dependent W_2 factor derived by Stenflo (1980). The frequency-dependent $W_2(\nu)$ contains the quantum interference effects and

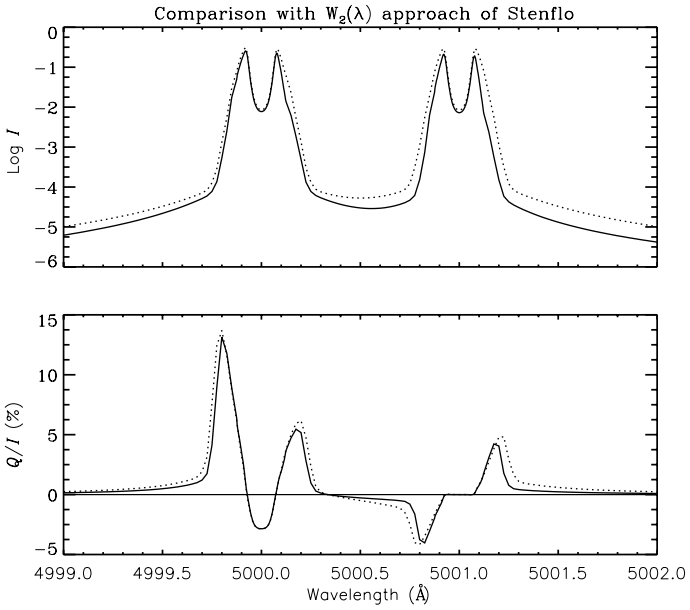

Fig. 7. Same as Fig. 3 but with the solid line computed using the redistribution matrix approach and the dotted line computed with the quantum interference theory that uses a wavelength-dependent $W_2(\lambda)$ factor. The model parameters are ($T = 2 \times 10^4, a = 10^{-3}, \epsilon = 10^{-4}, r = 0$).

is given by the formula (see Eq. (19) of Stenflo 1997)

$$W_2(\nu) = \frac{(\nu_2 - \nu)^{-2} + 2(\nu_1 - \nu)^{-1}(\nu_2 - \nu)^{-1}}{(\nu_1 - \nu)^{-2} + 2(\nu_2 - \nu)^{-2}}. \quad (34)$$

Thus we use $W_2(\nu)$ instead of a constant W_2. Also $\phi(x)$ is taken as the sum of the absorption profiles of the individual lines. From Eq. (34) one can see a double resonance at ν_1 and ν_2 and an interference in between these two resonances, which shows up in the emergent Q/I profiles shown in Fig. 7. Clearly, both these independent approaches give nearly the same results. The J-state interference effects along with PRD effects have been included in realistic modeling of the observed Q/I profiles of the Na I D_1 and D_2 lines by Fluri et al. (2003) based on the quantum interference theory of Stenflo (1980, 1997). Our results computed using the isothermal slab atmospheres show a similar behavior.

5. Conclusions

We presented the non-magnetic line transfer equation for a two-term atom including the effects of J-state interference for an arbitrary $L_a \rightarrow L_b \rightarrow L_a$ scattering transition. We showed that the decomposition technique of Frisch (2007) that was devised for a two-level atom case can be applied to the more difficult case of a two-term atom. This technique allows us to write a polarized approximate lambda iteration method to solve the concerned transfer problem. Numerical results were presented for a doublet taking the example of an $L = 0 \rightarrow 1 \rightarrow 0$ scattering transition with $S = 1/2$.

J-state interference produces asymmetric near wing PRD peaks around the center of the $1/2 \rightarrow 3/2 \rightarrow 1/2$ scattering transition. Also, anti-symmetric peaks are produced near the center of the $1/2 \rightarrow 1/2 \rightarrow 1/2$ transition. We showed that the J-state interference effects sensitively depend on the optical thickness of the medium. At the line core and near wings the variation of $(I, Q/I)$ with respect to various atmospheric parameters is similar to the behavior of a single line. The wavelength region in between the two lines is somewhat insensitive to the variation in ϵ for $T = 2 \times 10^4$. In the presence of a strong background continuum the PRD as well as J-state interference effects become suppressed. Finally, as the line separation (fine structure splitting) increases, the J-state interference effects decrease strongly as one moves away from the $1/2 \rightarrow 3/2 \rightarrow 1/2$ transition at 5000 Å.

The present extension of polarized radiative transfer theory to include two-term atoms with J-state interference is a significant step in our program to develop the theoretical tools that are needed to interpret the wealth of polarized structures that are observed in the second solar spectrum, so that they can be used to diagnose the magnetized solar atmosphere in ways not accessible by other means.

Acknowledgements. We thank the referee for useful comments and suggestions that helped to improve the paper. We would like to thank Ms. L. S. Anusha for useful discussions.

References

Bommier, V. 1997, A&A, 328, 726
Casini, R., & Manso Sainz, R. 2005 ApJ, 624, 1025
Chandrasekhar, S. 1950, Radiative Transfer (Oxford: Clarendon)
Faurobert-Scholl, M. 1991, A&A, 246, 469
Faurobert-Scholl, M., Frisch, H., & Nagendra, K. N. 1997, A&A, 322, 896
Fluri, D. M., Holzreuter, R., Klement, J., & Stenflo, J. O. 2003, in Solar Polarization 3, ed. J. Trujillo-Bueno, & J. Sanchez Almeida (San Francisco: ASP), ASP Conf. Ser., 307, 263
Frisch, H. 2007, A&A, 476, 665
Holzreuter, R., Fluri, D. M., & Stenflo, J. O. 2006, A&A, 449, L41
Hummer, D. G. 1962, MNRAS, 125, 21
Landi Degl'Innocenti, E. 1984, Sol. Phys., 91, 1
Landi Degl'Innocenti, E., & Landolfi, M. 2004, Polarization in Spectral Lines (Dordrecht: Kluwer) (LL04)
Landi Degl'Innocenti, E., Landi Degl'Innocenti, M., & Landolfi, M. 1997, in Proc. Forum THÉMIS, Science with THÉMIS, ed. N. Mein, & S. Sahal-Bréchot (Paris: Obs. Paris-Meudon), 59
Mihalas, D. 1978, Stellar Atmospheres (San Francisco: Freeman)
Manso Sainz, R., & Trujillo Bueno, J. 2003, in Solar Polarization 3, ed. J. Trujillo-Bueno, & Jorge Sanchez Almeida (San Francisco: ASP), ASP Conf. Ser., 301, 251
Manso Sainz, R., & Trujillo Bueno, J. 2010, ApJ, 722, 1416
Nagendra, K. N. 2003a, in Stellar Atmosphere Modeling, ed. I. Hubeny, D. Mihalas, & K. Werner (San Francisco: ASP) ASP Conf. Ser., 288, 583
Nagendra, K. N. 2003b, in Stellar Atmosphere Modeling, ed. I. Hubeny, D. Mihalas, & K. Werner (San Francisco: ASP) ASP Conf. Ser., 288, 611
Nagendra, K. N., & Sampoorna, M. 2009, in Solar Polarization 5, ed. S. V. Berdyugina, K. N. Nagendra, & R. Ramelli (San Francisco: ASP), ASP Conf. Ser., 405, 261
Nagendra, K. N., Frisch, H., & Faurobert, M. 2002, A&A, 395, 305
Nagendra, K. N., Anusha, L. S., & Sampoorna, M. 2009, Mem. S. A. It., 80, 678
Olson, G. L., Auer, L. H., & Buchler, J. R. 1986, J. Quant. Spec. Radiat. Transf., 35, 431
Paletou, F., & Auer, L. H. 1995, A&A, 297, 771
Rees, D. E. 1978, PASJ, 30, 455
Rees, D. E., & Saliba, G. J. 1982, A&A, 115, 1
Sampoorna, M., Nagendra, K. N., & Frisch, H. 2008, J. Quant. Spec. Radiat. Transf., 109, 2349
Sampoorna, M., Nagendra, K. N., & Frisch, H. 2011, A&A, 587, A89
Smitha, H. N., Sampoorna, M., Nagendra, K. N., & Stenflo, J. O. 2011, ApJ, 733, 4 (P1)
Stenflo, J. O. 1980, A&A, 84, 68
Stenflo, J. O. 1994, Solar Magnetic Fields: Polarized Radiation Diagnostics (Dordrecht: Kluwer)
Stenflo, J. O. 1997, A&A, 324, 344
Trujillo Bueno, J. 2003, in Stellar Atmosphere Modeling, ed. I. Hubeny, D. Mihalas, & K. Werner (San Francisco: ASP), ASP Conf. Ser., 288, 551
Trujillo Bueno, J. 2011, in Solar Polarization 6, ed. J. R. Kuhn, S. V. Berdyugina, D. M. Harrington, S. L. Keil, H. Lin, T. Rimmele, & J. Trujillo-Bueno (San Francisco: ASP), 437, 83
Trujillo Bueno, J., & Landi Degl'Innocenti, E. 1997, ApJ, 482, L183
Trujillo Bueno, J., Casini, R., Landolfi, M., & Landi Degl'Innocenti, E. 2002, ApJ, 566, L53